# Hyperspectral Band Selection via Spatial-Spectral Weighted Region-wise Multiple Graph Fusion-Based Spectral Clustering

**Chang Tang**[1] , **Xinwang Liu**[2*] , **En Zhu**[2] , **Lizhe Wang**[1*] , **Albert Zomaya**[3]
[1]School of Computer Science, China University of Geosciences, Wuhan 430074, China
[2]School of Computer, National University of Defense Technology, Changsha 410073, China
[3]School of Information Technologies, University of Sydney, NSW 2006, Australia
tangchang@cug.edu.cn, xinwangliu@nudt.edu.cn, lizhe.wang@gmail.com

## Abstract

In this paper, we propose a hyperspectral band selection method via spatial-spectral weighted region-wise multiple graph fusion-based spectral clustering, referred to as RMGF briefly. Considering that different objects have different reflection characteristics, we use a superpixel segmentation algorithm to segment the first principal component of original hyperspectral image cube into homogeneous regions. For each superpixel, we construct a corresponding similarity graph to reflect the similarity between band pairs. Then, a multiple graph diffusion strategy with theoretical convergence guarantee is designed to learn a unified graph for partitioning the whole hyperspectral cube into several subcubes via spectral clustering. During the graph diffusion process, the spatial and spectral information of each superpixel are embedded to make spatial/spectral similar superpixels contribute more to each other. Finally, the band containing minimum noise in each subcube is selected to represent the whole subcube. Extensive experiments are conducted on three public datasets to validate the superiority of the proposed method when compared with other state-of-the-art ones.
https://github.com/ChangTang/RMGF

## 1 Introduction

With the rapid development of hyperspectral remote sensing imaging technology, a large number of hyperspectral images (HSIs) are obtained. Compared to traditional RGB images, HSIs contain more abundant information about land cover objects since a HSI cube consists of hundreds of spectral bands, which record the reflectance of the scene by using different electromagnetic waves [Goetz, 2009]. Therefore, it is widely used in many fields, such as environmental monitoring, vegetation coverage estimation, and landslide detection. However, there are also non-negligible redundant information and noisy bands mixed in original HSI cube, which not only degenerate the performance but also induce high computational complexity of subsequent hyperspectral image analysis. As a result, it is necessary to reduce the redundant and noisy bands.

In the past decades, there are mainly two kinds of approaches proposed for HSI band dimension reduction, i.e., feature extraction and band section [Sun and Du, 2019]. As to the former one, original high-dimensional spatial data are often projected into a new feature space with lower dimension based on certain criteria. The criteria are designed to learn more discriminative features in the new feature space. The typical methods include linear discriminant analysis (LDA) [Bandos *et al.*, 2009], principal component analysis (PCA) [Chang *et al.*, 1999], independent component analysis (ICA) [Du *et al.*, 2003], and maximum noise fraction [Green *et al.*, 1988]. However, the physical meaning of the new feature space obtained through feature projection is not clear. For the latter, a subset of bands are selected from original data. The selected bands are required to be distinctive and representative based on some learning algorithms. In such a manner, the inherent band properties and physical meaning can be preserved. In this work, we also focus on band selection [Wang *et al.*, 2019].

Based on the availability of sample labels, existing band selection methods can be categorized into supervised ones [Feng *et al.*, 2014; Cao *et al.*, 2019] and unsupervised ones [Jia *et al.*, 2012; Yuan *et al.*, 2016]. For supervised methods, they need sample labels to train a classifier to select the most optimal bands. In addition, the appropriate training model is hard to design and sufficient labels are not easy to obtain. Compared to supervised methods, unsupervised ones are more flexible since they do not need the sample labels which are not available in practice in most cases. For unsupervised methods, they just need certain prior of original HSI data to construct leaning models with certain criteria such as information divergence [MartÍnez-UsÓMartinez-Uso *et al.*, 2007], sample similarity [Keshava, 2004], maximum ellipsoid volume [Geng *et al.*, 2014], etc.

For unsupervised hyperspectral band selection, clustering and ranking are two commonly used strategies. Ranking-based methods consists of two steps, i.e., evaluating the importance of each band and than select the most important bands. Typical evaluation criteria include information entropy [Guo *et al.*, 2006], information divergence [Chang and Wang, 2006] and maximum variance [Chang *et al.*, 1999]. As a kind of typical unsupervised leaning, clustering

*Corresponding Authors

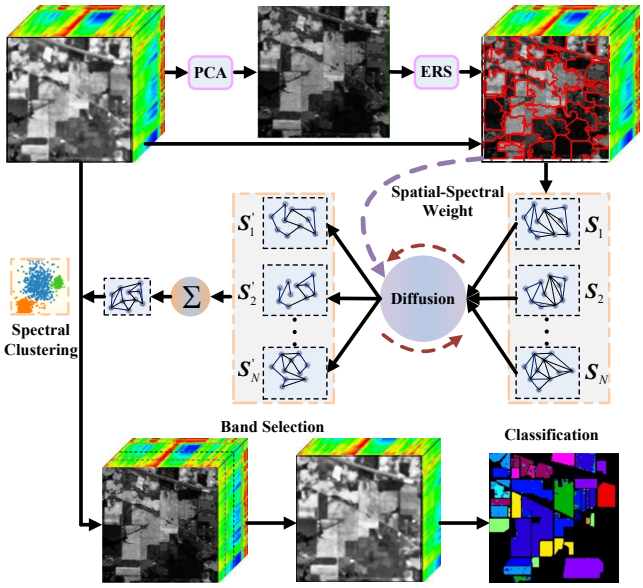


Figure 1: Flowchart of our hyperspectral band selection method via region-wise multiple graph fusion-based spectral clustering.

is widely used for hyperspectral band selection in the past few years and obtain satisfying results [Yuan *et al.*, 2015; Zhang *et al.*, 2017; Wang *et al.*, 2018; Li *et al.*, 2019; Wang *et al.*, 2019; 2020a]. Clustering based methods first partition original bands into several groups, then the optimal band of each group is selected to form the new band subset for subsequent tasks. Therefore, the clustering performance is critical for final results.

However, there are still at least two issues that hinder the band selection performance. Firstly, most of existing clustering based methods only take the correlation between neighbouring bands into account, while neglect the global information. Secondly, most of previous methods regard a certain band as a whole and reshape it to a feature vector, while the different reflection characteristics of objects are not exploited. In this paper, in order to tackle these two issues, we propose a hyperspectral band selection method via region-wise multiple graph fusion-based spectral clustering (RMGF). Since different objects are with different reflection characteristics, we first segment the first principal component of original hyperspectral image cube into homogeneous regions by using a certain superpixel segmentation, then we construct a similarity graph to reflect the similarity between band pairs corresponding to each region. For each region-wise graph, we design a diffusion process to update it to approximate the unified graph that reflects the global similarity between different bands. During the diffusion process, the spatial and spectral distribution of different superpixels are taken consideration, i.e., spatially adjacent superpixels should contribute more to each other. Finally, an optimal similarity graph is generated by using the multiple updated graphs and spectral clustering is performed to obtain different band partitions for band selection.

In a nutshell, the main contributions of this work are summarized as follows:

- As far as we know, this is the first work that proposes to fuse multiple graphs for clustering based hyperspectral band selection.
- Instead of treating a certain hyperspectral band as a whole to calculate the similarities between band pairs, we segment the hyperspectral band into homogeneous regions by considering that different objects are often with different reflection characteristics.
- We design a graph diffusion strategy to fuse multiple graphs for learning a consensus similarity graph that reflects the global relationship of all the hyperspectral bands. Extensive experiments are conducted to demonstrate the superiority of our proposed method when compared with other state-of-the-art hyperspectral band selection methods.

## 2 Related Work

In this section, we introduce some related clustering-based hyperspectral band selection methods which our proposed method belongs to.

For clustering-based methods, each band is treated as a data point and all of the bands are partitioned into several groups. Then, for each group, the most representative band is selected to form a new band subset. Based on the hierarchical clustering structure, MartÍnez-UsÓMartinez-Uso et al. [MartÍnez-UsÓMartinez-Uso *et al.*, 2007] proposed to select informative bands by minimizing the intra-class variance as well as maximizing the inter-class variance. In [Wang *et al.*, 2018], the dynamic programming is used for hyperspectral band partition. By estimating the band noise, the band with minimum noise in each group is selected as the representative band [Wang *et al.*, 2019]. In order to determine the appropriate number of selected bands, the context information is utilized with a fast neighborhood grouping method for hyperspectral band partition in a coarse to fine manner [Wang *et al.*, 2020a]. In [Yuan *et al.*, 2015], a novel descriptor is designed to reveal the context of HSI and a dual clustering method which includes the contextual information is proposed for band clustering. [Li *et al.*, 2019]. Based on the concept of shared nearest neighbor, the local density of each band and the information entropy are combined to select the optimal band subset.

Although great success has been achieved by previous clustering-based hyperspectral band selection methods, the global information as well as the spatial distribution of objects with different reflection characteristics are not well taken into consideration, which induces unsatisfactory results. Following we will introduce our proposed method to handle these issues in detail.

## 3 Proposed Methodology

In this section, the detailed process of our proposed RMGF will be elaborated step by step. In summary, RMGF consists of four main parts, i.e., homogeneous region segmentation, region-wise similarity graph construction, similarity graph diffusion and spectral-clustering based band selection, as shown in Figure 1.

### 3.1 Homogeneous Region Segmentation

In most of previous band selection methods, the spectral value of different pixels in a certain band are often stacked to form a single feature vector for band selection. However, it is well known that different objects are often with different reflection characteristics. Therefore, different homogeneous regions in hyperspectral images should be treated differently. In this work, we segment hyperspectral volume into several homogeneous regions with each region representing a certain object. Considering the promising performance in both efficacy and efficiency, we adopt the entropy rate superpixel segmentation (ESR) method [Liu *et al.*, 2011] to generate multiple homogeneous regions. Of course, other segmentation algorithms can also be used. Given a hyperspectral cube with size $H \times W \times B$ which consists of $B$ bands, in order to capture the major information of hyperspectral as well as reduce the computational cost, we first obtain the first principal component (denoted as $\mathbf{H}_f$) of the hyperspectral images by using principal component analysis (PCA) [Wold *et al.*, 1987]. Then, we can generate $N$ superpixels by performing ESR on $\mathbf{H}_f$ as follows:

$$\mathbf{H}_f = \bigcup_{p}^{N} \mathcal{R}_p, \quad s.t. \quad R_p \cap R_q = \emptyset, \quad (q \neq p), \tag{1}$$

where $\mathcal{R}_p$ is the $p$-th superpixel.

### 3.2 Region-wise Similarity Graph Construction

Based on the segmentation result of, for each superpixel, we can obtain corresponding multiple superpixels from different band which share the same pixel locations as the one in $\mathbf{H}_f$. Then we can calculate the similarity between each superpixel pair that represent the same homogeneous region across different bands. In such a manner, a $B \times B$ similarity graph which reflects the similarity of different bands in terms of each region can be obtained. Specifically, supposing that the feature vector represents the spectral values of the $p$-th superpixel in the $i$-th band and $j$-th band can be denoted as $\mathbf{x}_p^i$ and $\mathbf{x}_p^j$, respectively, then the $p$-th similarity graph can be calculated as follows:

$$\mathbf{S}_p(i,j) = \begin{cases} \exp(\frac{||\mathbf{x}_p^i - \mathbf{x}_p^j||^2}{-2\sigma^2}), & \mathbf{x}_p^i \in \mathcal{N}_k(\mathbf{x}_p^j) \ or \ \mathbf{x}_p^j \in \mathcal{N}_k(\mathbf{x}_p^i), \\ 0, & otherwise, \end{cases} \tag{2}$$

where $\mathcal{N}_k(\mathbf{x}_p^j)$ denotes the set of $k$ nearest neighbors of $\mathbf{x}_p^j$ and $\sigma$ is the kernel width of the Gaussian kernel function. Note that other distance measuring functions or learning strategies can be also used in Eq. (2) for calculating the similarity values. However, they are not our focus in this work and we just use the Euclidean distance for its simplicity and efficiency.

### 3.3 Similarity Graph Diffusion

Since there may be inaccurate values in the similarity graphs as obtained by Eq. (2), while there are often multiple superpixels which represent the same or similar object classes. Therefore, we design a diffusion strategy to update the initial similarity graphs by exploiting the supplementary information implied in different graphs [Tang *et al.*, 2020].

Given an initial $M \times M$ similarity graph $\mathbf{S}$ which indicates the similarities between $M$ sample points, a more faithful similarity graph $\bar{\mathbf{S}}$ can be learned via diffusion process. As indicated by the manifold ranking model [Zhou *et al.*, 2004; Bai *et al.*, 2017], we can obtain the new similarity graph $\bar{\mathbf{S}}$ by solving the following optimization problem:

$$\begin{aligned} \min_{\bar{\mathbf{S}}} \frac{1}{2} \sum_{i,j=1}^{M} \sum_{p,q=1}^{M} \mathbf{S}_{ij}\mathbf{S}_{pq} \left( \frac{\bar{\mathbf{S}}_{ip}}{\sqrt{\mathbf{D}_{ii}\mathbf{D}_{pp}}} - \frac{\bar{\mathbf{S}}_{jq}}{\sqrt{\mathbf{D}_{jj}\mathbf{D}_{qq}}} \right)^2 \\ + \mu \sum_{i,j=1}^{N} (\bar{\mathbf{S}}_{ij} - \mathbf{S}_{ij})^2, \end{aligned} \tag{3}$$

where $\mu > 0$ is a regularization parameter. $\mathbf{D}$ is a diagonal degree matrix with its $i$-th diagonal elements $\mathbf{D}_{ii} = \sum_{j=1}^{M} \mathbf{S}_{ij}$. As can be seen from Eq. (3), it consists of two terms. The first term is the analogy to local and global consistency [Zhou *et al.*, 2003] which regularizes that if data point $i$ is similar to data point $j$ and data point $p$ is also similar to data point $q$ on original similarity graph $S$, then the learned new similarities $\bar{\mathbf{S}}_{ip}$ and $\bar{\mathbf{S}}_{jq}$ should also be similar. The second term can be regarded as a fitting term which regularizes that that a good learned similarity graph should not change too much from its initial status.

As derived in [Bai *et al.*, 2017], Eq. (3) has a closed-form solution as follows:

$$\bar{\mathbf{S}} = (1-\alpha) vec^{-1}((\mathbf{I} - \alpha\mathbb{A})^{-1} vec(\mathbf{F})), \tag{4}$$

where $\alpha = \frac{1}{1+\mu}$. $vec(\cdot)$ is an operator which vectorizes an input matrix by stacking its columns one by one and the corresponding inverse operator is denoted as $vec(\cdot)^{-1}$. $\mathbb{A} \in \mathbb{R}^{M^2 \times M^2}$ is the Kronecker product of $\mathbf{A}$, i.e., $\mathbf{A} \otimes \mathbf{A}$ with $\mathbf{A} = \mathbf{D}^{-\frac{1}{2}}\mathbf{S}\mathbf{D}^{-\frac{1}{2}}$.

Motivated by the previous works [Donoser and Bischof, 2013] that run in an iterative manner, the iteratively similarity propagation can be also formulated as follows:

$$\bar{\mathbf{S}}^{(t+1)} = \alpha\mathbf{A}\bar{\mathbf{S}}^{(t)}\mathbf{A}^T + (1-\alpha)\mathbf{S}, \tag{5}$$

where $t$ represents the $t$-th iteration time.

Eq. (5) has a obvious drawback since it can only update a single similarity graph. In this work, we design a diffusion strategy to update the multiple graphs corresponding to multiple regions of hyperspectral images by fully exploiting the complementarity among different graphs.

In a certain band of the hyperspectral images, the superpixels with similar spectral values or closer spatial locations are more likely to represent the same objects. Therefore, during the diffusion process, the similarity graphs corresponding to superpixels which are with similar spectral values as well as closer spatial locations should contribute more to each other. With this point in mind, for the similarity graph of the $p$-th superpixel, we design the diffusion process to update $\mathbf{S}_p$ as follows:

$$\mathbf{S}_p^{(t+1)} = \alpha\mathbf{A}_p^t \cdot \left( \frac{1}{N-1} \sum_{\substack{q=1 \\ q \neq p}}^{N} \omega_{pq}\mathbf{S}_q^{(t)} \right) \cdot (\mathbf{A}_p^t)^T + (1-\alpha)\mathbf{S}_p, \tag{6}$$

where $\alpha$ is a parameter to balance the updated graph and its initial status. In our experiments, on order to emphasize the updated graph, we empirically set $\alpha = 0.7$. $\omega_{pq}$ denotes the weight that the $q$-th graph contributes to the $p$-th graph, which can be defined as follows:

$$\omega_{pq} = \frac{\exp(\frac{||\mathbf{x}_p - \mathbf{x}_q||^2}{-2{\sigma_{sv}}^2})}{\sum_{p,q=1}^{N} \exp(\frac{||\mathbf{x}_p - \mathbf{x}_q||^2}{-2{\sigma_{sv}}^2})} + \frac{\exp(\frac{||\mathbf{l}_p - \mathbf{l}_q||^2}{-2{\sigma_{sl}}^2})}{\sum_{p,q=1}^{N} \exp(\frac{||\mathbf{l}_p - \mathbf{l}_q||^2}{-2{\sigma_{sl}}^2})}, \tag{7}$$

where $\mathbf{x}_p$ and $\mathbf{x}_q$ denote the $p$-th and $q$-th feature vector of the corresponding superpixel in the the first principal component (i.e., $\mathbf{H}_f$) of the hyperspectral images as introduced in previous section. $\mathbf{l}_p$ and $\mathbf{l}_q$ denote the center pixel location of the $p$-th and $q$-th superpixel in $\mathbf{H}_f$. $\sigma_{sv}$ and $\sigma_{sl}$ are two parameters that control the spectral sensitivity and spatial sensitivity of the element distribution, respectively. In Eq. (7), the first term measures the spectral similarity of two superpixels while the second term measures the spatial distance of two superpixels.

By using Eq. (6), the connection information in different graphs can be interchanged iteratively to achieve the final unified graph. On one hand, similarity values of different similarity graphs are propagated to each other by the iterative diffusion process. On the other hand, the information from original similarity graphs are partially preserved by the scalar parameter $\alpha$. In addition, the spectral and spatial similarity of different superpixels are used to weight the diffusion process for better exploiting the complementarity among multiple graphs.

After $T$ times of diffusion, each single similarity graph corresponding to a superpixel can be updated to a stable status. Then the final unified graph which reflects the similarity of different hyperspectral bands can be obtained as follows:

$$\mathbf{S}^* = \frac{1}{N} \sum_{p=1}^{N} \mathbf{S}_p^{(T)}, \tag{8}$$

which is used for final spectral clustering to partition original hyperspectral bands into several band subsets.

### 3.4 Spectral-clustering Based Band Selection

Given a certain number of bands $K$ that we want to select, original hyperspectral bands can be partitioned to $K$ subsets by performing spectral clustering algorithm on $\mathbf{S}^*$. As to each band subset, the band which is closest to the subset center is selected as the representative band.

### 3.5 Theoretical Analysis of the Diffusion Process

#### Computational Complexity Analysis

As can be seen from Eq. (6), after we obtain the initial similarity graphs of different superpixels, the major computational cost of each diffusion iteration is the multiplication operation of matrices with size $B \times B$, of which the computational time complexity is $\mathcal{O}(B^3)$. Therefore, the whole computational time complexity of the diffusion process is $\mathcal{O}(TB^3)$, where $T$ is the final iteration times.

#### Theoretical Convergence Analysis

In this section, we give the theoretical convergence analysis of the iterative diffusion process. Similar to [Bai *et al.*, 2017], we firstly introduce the following Lemma 1.

**Lemma 1.** *Given three matrices $\boldsymbol{X}$, $\boldsymbol{Y}$ and $\boldsymbol{Z}$ with appropriate sizes, then* $vec(\boldsymbol{XYZ}^T) = (\boldsymbol{Z} \otimes \boldsymbol{X})vec(\boldsymbol{Y})$.

By applying $vec(\cdot)$ to both sides of Eq. (6), we have

$$\begin{aligned} vec(\mathbf{S}_p^{(t+1)}) &= \alpha \mathbb{A} vec(\mathbf{Q}_p^{(t)}) + (1-\alpha) vec(\mathbf{S}_p) \\ &= (\alpha\mathbb{A})^t vec(\mathbf{S}_p^{(1)}) + (1-\alpha) \sum_{k=0}^{t-1} (\alpha\mathbb{A})^k vec(\mathbf{S}_p) \end{aligned} \tag{9}$$

where $\mathbf{Q}_p^{(t)} = \frac{1}{N-1} \sum_{q=1, q\neq p}^{N} \omega_{pq} \mathbf{S}_q^{(t)}$.

Since the spectral radius of $\mathbf{A}$ is no larger than 1, according to the properties of Kronecker product, the eigenvalues of $\mathbb{A} = \mathbf{A} \otimes \mathbf{A}$ are also in $[-1, 1]$. Since $0 < \alpha < 1$, we have

$$\begin{cases} \lim\limits_{t\to\infty} (\alpha\mathbb{A})^t vec(\mathbf{Q}_p^{(1)}) = 0 \\ \lim\limits_{t\to\infty} \sum\limits_{k=0}^{t-1} (\alpha\mathbb{A})^k vec(\mathbf{S}_p^{(1)}) = (\mathbf{I} - \alpha\mathbb{A})^{-1} vec(\mathbf{S}_p^{(1)}). \end{cases} \tag{10}$$

Therefore, when $t \to \infty$, Eq. (9) converges as

$$\lim_{t\to\infty} vec(\mathbf{S}_p^{(t+1)}) = (1-\alpha)(\mathbf{I} - \alpha\mathbb{A})^{-1} vec(\mathbf{S}_p^{(1)}). \tag{11}$$

By applying $vec^{-1}$ to both sides of Eq. (11), the iteration converges to exactly the same solution in Eq. (4).

## 4 Experiments

In this section, extensive experiments are conducted on three commonly used public hyperspectral image datasets to demonstrate the efficacy of the proposed method.

### 4.1 Datasets

Three datasets include Indian Pines scene, Pavia University Scene and Salinas Scene are used for our experiments. The detailed information are as follows.

**Indian Pines Scene:** This dataset was collected by the AVIRIS sensor in 1992, which consists of 224 spectral bands with the size of $145 \times 145$ pixels from 0.4 to 2.5$\mu$m. There are 16 different classes of land cover objects in the scene. Since some bands (104–108, 150–163, and 220) are with heavy noises due to water absorption, we discard those noisy bands and finally fetch 200 bands for experiments.

**Pavia University Scene:** This dataset was captured over Pavia by the ROSIS sensor in 2002. Similar to the Indian Pines dataset, after removing some noisy bands, 103 spectral bands are remained. The size of each band is $610$ and there are 9 classes of land cover objects in this scene.

**Salinas Scene:** This dataset was also gathered by the AVIRIS sensor over Salinas Valley, CA, USA, in 1998. This dataset is with a high spatial resolution (3.7-m pixels) and has a total of 224 spectral bands with the size of $512 \times 217$. There are 16 classes of land cover objects in this scene.

| Datasets | Classifiers | UBS | TOF | ASPS_MN | ASPS_IE | FNGBS | ONR | RMGF |
|---|---|---|---|---|---|---|---|---|
| Indian Pines | KNN | 66.40±0.17 | 68.55±0.14 | 70.92±0.12 | 71.34± 0.12 | 71.48±0.14 | 69.98±0.26 | **76.26±0.16** |
| | SVM | 80.09±0.16 | 79.48±0.17 | 81.20±0.25 | 81.26± 0.16 | 81.77±0.17 | 80.25±0.37 | **86.48±0.17** |
| | LDA | 71.12±0.18 | 70.90±0.10 | 70.46±0.32 | 70.20± 0.22 | 70.52±0.16 | 70.09±0.20 | **81.19±0.12** |
| Pavia University | KNN | 86.43±0.07 | 86.00±0.04 | 87.28±0.15 | 87.07±0.06 | 87.36±0.05 | 89.10±0.15 | **91.76±0.13** |
| | SVM | 94.33±0.05 | 94.10±0.02 | 94.08±0.26 | 93.95± 0.14 | 94.46±0.07 | 94.27±0.14 | **96.35±0.09** |
| | LDA | 84.19±0.06 | 84.16±0.08 | 84.06±0.16 | 83.62±0.09 | 84.20±0.04 | 83.48±0.13 | **90.49±0.07** |
| Salinas | KNN | 89.33±0.03 | 88.95±0.05 | 89.38±0.14 | 89.14±0.04 | 89.24±0.05 | 89.33± 0.13 | **92.35±0.12** |
| | SVM | 93.26±0.04 | 93.46±0.04 | 93.13±0.15 | 93.08± 0.05 | 93.25±0.06 | 93.35±0.16 | **95.00±0.11** |
| | LDA | 90.41±0.04 | 90.31±0.03 | 90.30±0.06 | 89.93±0.02 | 90.37±0.03 | 90.69±0.15 | **92.32±0.08** |

Table 1: The OA and corresponding standard deviation of different band selection methods with different classifiers on three datasets. The best results are highlighted in bold font.

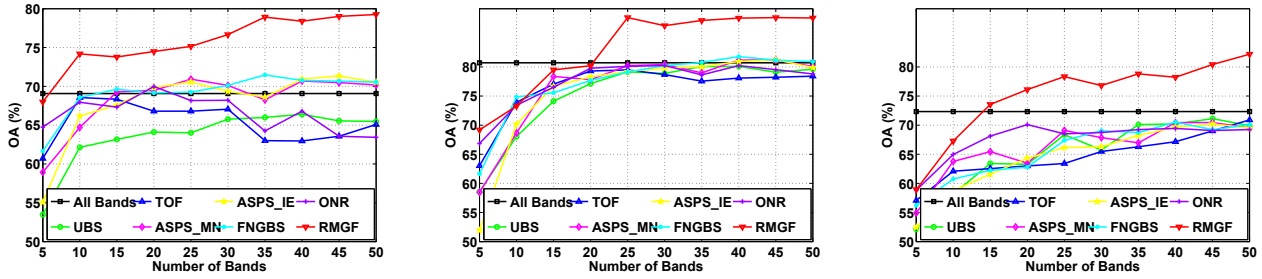


(a) (b) (c)

Figure 2: OA of three classifiers by varying the number of selected bands on the Indian Pines dataset. (a) OA obtained by KNN. (b) OA obtained by SVM. (c) OA obtained by LDA.

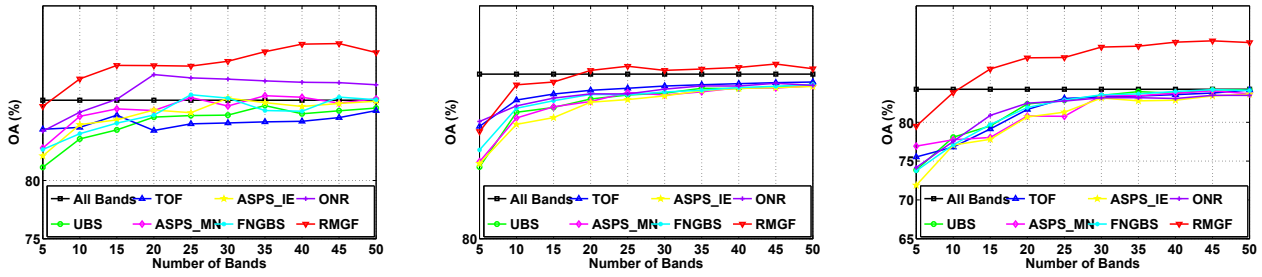


(a) (b) (c)

Figure 3: OA of three classifiers by varying the number of selected bands on the Pavia University dataset. (a) OA obtained by KNN. (b) OA obtained by SVM. (c) OA obtained by LDA.

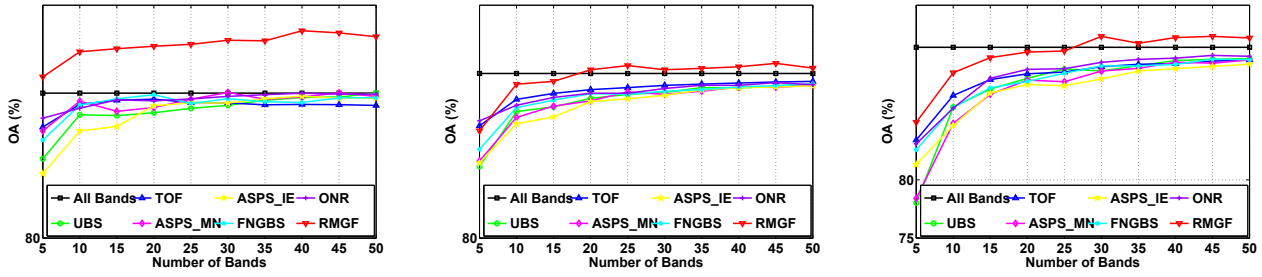


(a) (b) (c)

Figure 4: OA of three classifiers by varying the number of selected bands on the Salinas dataset. (a) OA obtained by KNN. (b) OA obtained by SVM. (c) OA obtained by LDA.

### 4.2 Compared Methods

In order to validate the superiority of our proposed RMGF, five other unsupervised hyperspectral band selection methods are used for comparison, they are as follows:
1) UBS [Chang and Wang, 2006], which divides the hyperspectral image cube into multiple subcubes at equal width based on the required number of selected bands, each segmentation point is viewed as the representative band.
2) TOF [Wang *et al.*, 2018], which aims to construct an optimal clustering model with rank constraint to provide an effective criterion for selecting bands on existing clustering structure.
3) ASPS_MN [Wang *et al.*, 2019], which performs hyperspectral band selection via an adaptive subspace partition strategy. The representative band of each band subset is selected based on band noise estimation.
4) ASPS_IE [Wang *et al.*, 2019], similar to ASPS_MN that selects representative bands from band subsets, but it differs to ASPS_MN that the representative band of each band subset is selected by the information entropy.
5) FNGBS [Wang *et al.*, 2020a], which is a fast neighborhood grouping method for hyperspectral band selection. The band with the highest local density and information entropy of each band subset is selected.
6) ONR [Wang *et al.*, 2020b], which selects those bands that are with high capability to reconstruct other bands and formulates the band selection as a combinatorial optimization problem.

### 4.3 Experimental Setup

In our experiments, three typical classifiers, including $k$-nearest neighborhood (KNN), support vector machine (SVM), and linear discriminant analysis (LDA), are used to evaluate the classification performance of different band selection algorithms. Since the desired number of selected bands is unknown and yet difficult to determine in practice for different datasets, we vary the number of selected bands from 5 to 60 with step 5 to illustrate the influence of different numbers of bands on the final classification accuracy. The parameter $k$ of KNN is set to 3 for all experiments. For the SVM classifier, we implement it with the RBF kernel, and the penalty $C$ and gamma are set 1e4 and 0.5, respectively.

For each dataset, 10% samples of each class are randomly chosen to construct the training set, and the rest 90% samples are used for testing. In addition, we perform each algorithm ten times and report the average results for reducing the influence of random selection of training and testing samples.

### 4.4 Experimental Results

In order to validate the efficacy of the proposed method, we compare it with other six state-of-the-art ones by using three different classifiers. By selecting the optimal number of selected bands, the overall accuracy (OA) of different methods on three different datasets are shown in Table 1. The best results are highlighted in bold font. As can be seen, our proposed RMGF consistently outperforms other competitors in terms of different classifiers on all of the three datasets.

As to the Indian Pines dataset, our RMGF obtains more than 7% OA when compared to other methods by using different classifiers. Specially, when using LDA as classifier, RMGF gains more than 10% OA. For Pavia University dataset, when using LDA as classifier, RMGF also obtains more than 5% improvement than other methods.

As aforementioned, it is difficult to determine the desired number of selected bands in practice for different datasets, we plot the OA curves for every five bands for each dataset in Figure 2-4. As can be seen, our proposed method outperforms other ones in most of the numbers of selected bands. As shown in Figure 2 and 3, by performing KNN and LDA on the selected bands of RMGF, we can always obtain higher OA on Indian Pines and Pavia University datasets. In Figure 4, we can see that RMGF can always select more discriminative bands for different classifiers.

## 5 Conclusion

In this paper, we present a hyperspectral band selection method via spatial-spectral weighted region-wise multiple graph fusion-based spectral clustering (RMGF). By considering that different objects have different reflection characteristics, we partition the hyperspectral images into multiple homogeneous regions, with each region representing the same class of object. For each region across different bands, we constructs a corresponding similarity graph to reflect the similarity between band pairs. Then, a spatial-spectral weighted multiple graph fusion strategy is designed to learn a unified graph for final band clustering. The optimal bands are selected based on the clustering results. Extensive experiments on three datasets are conducted to demonstrate the superiority of RMGF when compared with other state-of-the-art methods.

## Acknowledgements

The work was supported in part by the National Science Foundation (NSF) of China (No. 62076228); in part by National Key R&D Program of China (No. 2020AAA0107100); in part by Natural Natural Science Foundation of Hubei Province (No. 2020CFB644); in part by the Opening Fund of Key Laboratory of Geological Survey and Evaluation of Ministry of Education (No. GLAB2020ZR18) and the Fundamental Research Funds for the Central Universities; Sponsored by CAAI-Huawei MindSpore Open Fund, see [Huawei Technologies Co., 2020].

## References

[Bai *et al.*, 2017] Song Bai, Xiang Bai, Qi Tian, and Longin Jan Latecki. Regularized diffusion process for visual retrieval. In *AAAI*, pages 3967–3973, 2017.

[Bandos *et al.*, 2009] Tatyana V Bandos, Lorenzo Bruzzone, and Gustavo Camps-Valls. Classification of hyperspectral images with regularized linear discriminant analysis. *IEEE TGARS*, 47(3):862–873, 2009.

[Cao *et al.*, 2019] Xianghai Cao, Cuicui Wei, Yiming Ge, Jie Feng, Jing Zhao, and Licheng Jiao. Semi-supervised hyperspectral band selection based on dynamic classifier selection. *IEEE JSTARS*, 12(4):1289–1298, 2019.

[Chang and Wang, 2006] Chein-I Chang and Su Wang. Constrained band selection for hyperspectral imagery. *IEEE TGARS*, 44(6):1575–1585, 2006.

[Chang *et al.*, 1999] Chein-I Chang, Qian Du, Tzu-Lung Sun, and Mark LG Althouse. A joint band prioritization and band-decorrelation approach to band selection for hyperspectral image classification. *IEEE TGARS*, 37(6):2631–2641, 1999.

[Donoser and Bischof, 2013] Michael Donoser and Horst Bischof. Diffusion processes for retrieval revisited. In *CVPR*, pages 1320–1327, 2013.

[Du *et al.*, 2003] Hongtao Du, Hairong Qi, Xiaoling Wang, Rajeev Ramanath, and Wesley E Snyder. Band selection using independent component analysis for hyperspectral image processing. In *AIPRW*, pages 93–98. IEEE, 2003.

[Feng *et al.*, 2014] Jie Feng, Licheng Jiao, Fang Liu, Tao Sun, and Xiangrong Zhang. Mutual-information-based semi-supervised hyperspectral band selection with high discrimination, high information, and low redundancy. *IEEE TGARS*, 53(5):2956–2969, 2014.

[Geng *et al.*, 2014] Xiurui Geng, Kang Sun, Luyan Ji, and Yongchao Zhao. A fast volume-gradient-based band selection method for hyperspectral image. *IEEE TGARS*, 52(11):7111–7119, 2014.

[Goetz, 2009] Alexander FH Goetz. Three decades of hyperspectral remote sensing of the earth: A personal view. *Remote Sensing of Environment*, 113:S5–S16, 2009.

[Green *et al.*, 1988] Andrew A Green, Mark Berman, Paul Switzer, and Maurice D Craig. A transformation for ordering multispectral data in terms of image quality with implications for noise removal. *IEEE TGARS*, 26(1):65–74, 1988.

[Guo *et al.*, 2006] Baofeng Guo, Steve R Gunn, Robert I Damper, and James DB Nelson. Band selection for hyperspectral image classification using mutual information. *IEEE GRSL*, 3(4):522–526, 2006.

[Huawei Technologies Co., 2020] Ltd. Huawei Technologies Co. Mindspore. https://www.mindspore.cn/, 2020.

[Jia *et al.*, 2012] Sen Jia, Zhen Ji, Yuntao Qian, and Linlin Shen. Unsupervised band selection for hyperspectral imagery classification without manual band removal. *IEEE JSTARS*, 5(2):531–543, 2012.

[Keshava, 2004] Nirmal Keshava. Distance metrics and band selection in hyperspectral processing with applications to material identification and spectral libraries. *IEEE TGARS*, 42(7):1552–1565, 2004.

[Li *et al.*, 2019] Qiang Li, Qi Wang, and Xuelong Li. An efficient clustering method for hyperspectral optimal band selection via shared nearest neighbor. *Remote Sensing*, 11(3):350, 2019.

[Liu *et al.*, 2011] Ming-Yu Liu, Oncel Tuzel, Srikumar Ramalingam, and Rama Chellappa. Entropy rate superpixel segmentation. In *CVPR*, pages 2097–2104. IEEE, 2011.

[MartÍnez-UsÓMartinez-Uso *et al.*, 2007] Adolfo MartÍnez-UsÓMartinez-Uso, Filiberto Pla, José Martínez Sotoca, and Pedro García-Sevilla. Clustering-based hyperspectral band selection using information measures. *IEEE TGARS*, 45(12):4158–4171, 2007.

[Sun and Du, 2019] Weiwei Sun and Qian Du. Hyperspectral band selection: A review. *IEEE GRSM*, 7(2):118–139, 2019.

[Tang *et al.*, 2020] Chang Tang, Xinwang Liu, Xinzhong Zhu, En Zhu, Zhigang Luo, Lizhe Wang, and Wen Gao. Cgd: Multi-view clustering via cross-view graph diffusion. In *AAAI*, pages 5924–5931, 2020.

[Wang *et al.*, 2018] Qi Wang, Fahong Zhang, and Xuelong Li. Optimal clustering framework for hyperspectral band selection. *IEEE TGARS*, 56(10):5910–5922, 2018.

[Wang *et al.*, 2019] Qi Wang, Qiang Li, and Xuelong Li. Hyperspectral band selection via adaptive subspace partition strategy. *IEEE JSTARS*, 12(12):4940–4950, 2019.

[Wang *et al.*, 2020a] Qi Wang, Qiang Li, and Xuelong Li. A fast neighborhood grouping method for hyperspectral band selection. *IEEE TGARS*, 2020.

[Wang *et al.*, 2020b] Qi Wang, Fahong Zhang, and Xuelong Li. Hyperspectral band selection via optimal neighborhood reconstruction. *IEEE TGARS*, 2020.

[Wold *et al.*, 1987] Svante Wold, Kim Esbensen, and Paul Geladi. Principal component analysis. *CILS*, 2(1-3):37–52, 1987.

[Yuan *et al.*, 2015] Yuan Yuan, Jianzhe Lin, and Qi Wang. Dual-clustering-based hyperspectral band selection by contextual analysis. *IEEE TGARS*, 54(3):1431–1445, 2015.

[Yuan *et al.*, 2016] Yuan Yuan, Xiangtao Zheng, and Xiaoqiang Lu. Discovering diverse subset for unsupervised hyperspectral band selection. *IEEE TIP*, 26(1):51–64, 2016.

[Zhang *et al.*, 2017] Fahong Zhang, Qi Wang, and Xuelong Li. Hyperspectral image band selection via global optimal clustering. In *IGARSS*, pages 1–4. IEEE, 2017.

[Zhou *et al.*, 2003] Dengyong Zhou, Olivier Bousquet, Thomas Lal, Jason Weston, and Bernhard Schölkopf. Learning with local and global consistency. In *NIPS*, pages 321–328, 2003.

[Zhou *et al.*, 2004] Dengyong Zhou, Jason Weston, Arthur Gretton, Olivier Bousquet, and Bernhard Schölkopf. Ranking on data manifolds. In *NIPS*, pages 169–176, 2004.